JOURNAL OF SOLID STATE CHEMISTRY **140,** 307–315 (1998)
ARTICLE NO. SC987892

Neutron Diffraction and TEM Studies of the Crystal Structure and Defects of $Nd_4Ni_3O_8$

R. Retoux,*,[1] J. Rodriguez-Carvajal,† and P. Lacorre*

*Laboratoire des Fluorures, UPRES-A CNRS 6010, Université du Maine, 72085 Le Mans Cedex 9, France; and †Laboratoire Léon-Brillouin, CEA-CNRS, Centre d'Etudes de Saclay, 91191 Gif-sur-Yvette Cedex, France

Received February 27, 1998; accepted May 12, 1998

Powder neutron diffraction and electron microscopy studies confirmed the crystal structure of $Nd_4Ni_3O_8$ (space group $I4/mmm$; $a = b = 3.9168(2)$ Å, $c = 25.322(2)$ Å, $Z = 4$; reliability factors $R_p = 0.125$, $R_{wp} = 0.108$, $\chi^2 = 2.81$, $R_{Bragg} = 0.043$, $R_F = 0.037$) previously determined by powder X-ray diffraction [Ph. Lacorre, *J. Solid State Chem.* 97, 495 (1992)]. It consists in the intergrowth between triple layers of nickel in square planar coordination with Nd in cubic coordination (infinite layer type) and fluorite type layers. $Nd_4Ni_3O_8$ is thus the first known compound with a triple T′ type structure (relative to the single T′ type structure of Nd_2CuO_4). A study of the coherent diffraction lengths and defects in the structure has been carried out. Two kinds of defects have been detected by HREM, for which a model is proposed. © 1998 Academic Press

Key Words: **triple T′ structure; square planar coordination; monovalent and divalent nickel; Ni^{1+} and Ni^{2+} layered oxide; Ruddlesden–Popper series; electron microscopy; HREM: neutron powder diffraction; defects.**

1. INTRODUCTION

So-called T, T*, and T′ structures are typical structural arrangements of single-layer hole-doped and electron-doped superconducting cuprates, with copper in octahedral, pyramidal, and square planar coordination, respectively (see for instance Ref. (1)). In a previous article (2), one of us has shown the possibility of reducing significantly under hydrogen the triple layer nickelates belonging to the Ruddlesden–Popper type series $A_{n+1}B_nO_{3n+1}$ (3), i.e., triple T type (see Fig. 1a). Starting from $R_4Ni_3O_{10}$, (R = La, Pr, Nd), a definite composition was obtained with stoichiometry $R_4Ni_3O_8$, as deduced from TGA measurements. Powder X-ray diffraction showed that the reduction was accompanied by a drastic reduction of the cell parameter along the perovskite layers stacking, resulting from the loss of two apical oxygen atoms. This could result in a structural arrangement similar to that of $La_2Ca_2Cu_3O_8$ (4), with a T* type arrangement (see Fig. 1b). Nevertheless, X-ray diffraction suggested a migration of the remaining apical oxygen within the rock salt layers toward a position typical of the fluorite arrangement, leaving all nickel atoms in a square planar coordination, as compared to octahedral coordination in the parent oxidized compounds. This results in an unprecedented structural arrangement (Fig. 1c), similar to that of Nd_2CuO_4 (T′ type structure), but with three square planar layers in between fluorite type layers (instead of 1 in Nd_2CuO_4), namely a triple T′ type structure. However, the relatively low number of electrons of oxygen anions, especially when compared to that of rare earth cations, led us to check the anionic arrangement by means other than X-ray diffraction in order to confirm this. The aim of this article is to present the results of such a study on $Nd_4Ni_3O_8$, involving neutron diffraction and transmission electron microscopy (TEM). Special attention will be paid to the presence of defects observed in the structural arrangement of the compound.

2. EXPERIMENTAL

2.1. Synthesis

$Nd_4Ni_3O_8$ was prepared according to the procedure described in (2). The first step consists in the synthesis of the parent oxidized compound $Nd_4Ni_3O_{10}$, starting from a stoichiometric mixture of Nd_2O_3 and NiO, prepared by thermal decomposition of nitrates. The mixture was then pressed into pellets and fired at 950°C in flowing oxygen for several weeks, with several intermediate regrindings and pressings.

The second step corresponds to the reduction of the sample, for a few days at 320°C in flowing hydrogen.

2.2. Electron Microscopy

The HREM and ED studies were performed on a 200 kV side entry JEOL 2010 electron microscope (tilt ± 30°).

[1]To whom correspondence should be addressed. E-mail: Richard.Retoux@fluo.univ-lemans.fr.

0022-4596/98 $25.00

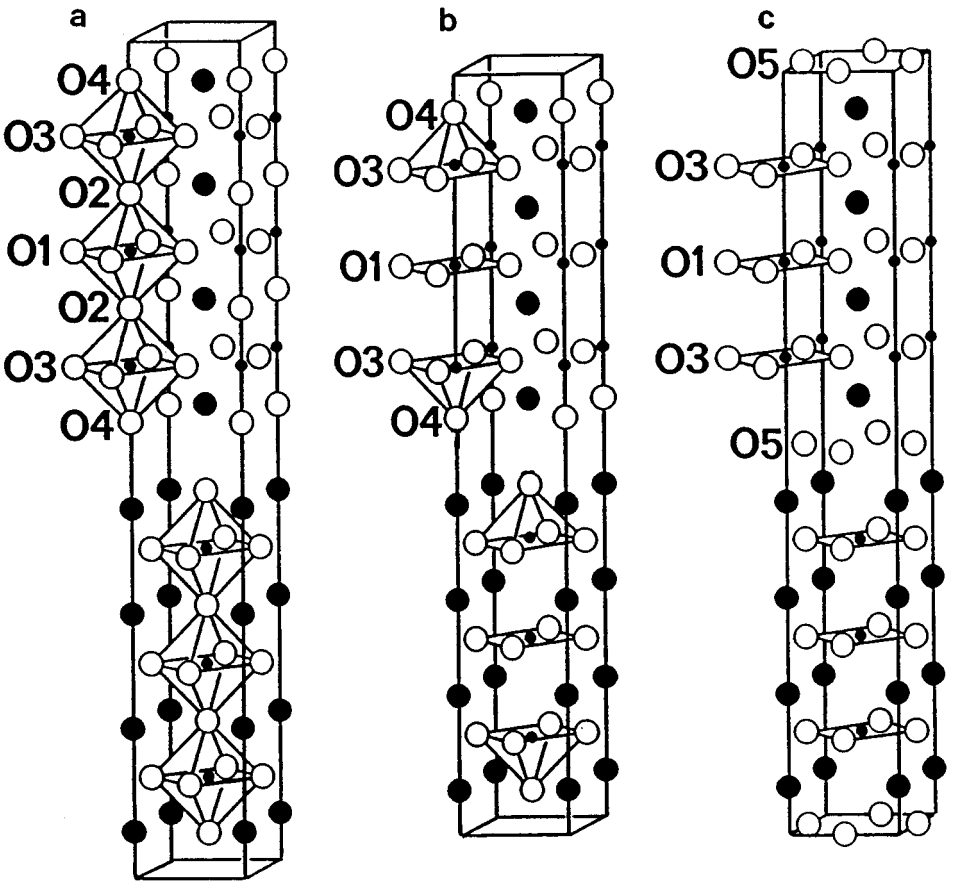

FIG. 1. (a) Crystal structure of $R_4Ni_3O_{10}$ (R = La, Pr, Nd): T type; (b) Possible crystal structure for the reduced forms: T* type; (c) Crystal structure of $R_4Ni_3O_8$ as suggested by X-ray diffraction (2): T′ type. (Atomic symbols: ● = Nd, • = Ni, ○ = O.)

Specimens for electron microscopy were prepared by suspending as much as possible thin crystals in alcohol (obtained from a thorough grinding of a powdered sample); a few droplets of the suspension were put on a carbon-coated holey film. In spite of this treatment, observations, particularly in high-resolution mode, were very difficult to make due to the thickness of the crystals. Only very small domains (a few nanometers wide) on crystal edges had thicknesses allowing high-resolution studies.

The series of programs written by P. A. Stadelman (5) were used to simulate high-resolution images at different focus using the multislice method (with $C_s = 1$, $\Delta_F = \pm 10$ Å) for different thickness of crystals.

2.3. *Powder Neutron Diffraction*

The powder neutron diffraction patterns were collected using the diffractometer D1A that was installed in the guide G4 of the Orphée reactor, at Laboratoire Léon Brillouin (Saclay, France), during the refurbishing of the Institut Laue-Langevin reactor. G4 is a cold neutron guide providing high flux for long-wavelength neutrons (2–6 Å). The diffraction pattern was recorded at room temperature with neutrons of wavelength 1.9845 Å emerging from a vertical focusing Ge(115) monochromator at a take-off angle of 135°. The measured angular range was 2–160° (2θ), with a 2θ step size of 0.05°. Low-temperature data were taken with the sample in a standard Orange cryostat in order to determine the magnetic structure. The results of the low-temperature measurements will be published elsewhere. The data analysis was performed using the program FullProf (6).

The peak shape of the Bragg reflections were well described using the pseudo-Voigt function in the form parametrized by Thompson, Cox, and Hasting (7). This peak shape allows quite a good treatment of microstructural (strain and size) effects. The resolution function of D1A is well accounted for by the full width at half maximum (FWHM) of the gaussian component of the true Voigt function (not to be confused with the FWHM of the pseudo-Voigt function). The lorentzian components are mainly due to size effects of the sample.

3. RESULTS

3.1. Electron Diffraction

The cell parameters and reflection conditions deduced from electron diffraction on crystals of $Nd_4Ni_3O_8$ are in agreement with space group $I4/mmm$ used in the X-ray diffraction study (2). The reflection conditions hkl ($h + k + l = 2n$) imply an I type group. The [001]*, [010]*, [110]* electron diffraction patterns of $Nd_4Ni_3O_8$ shown on Fig. 2 provide evidence for the $hk0$ ($h + k = 2n$), $0kl$ ($k + l = 2n$), and hhl ($l = 2n$) conditions, leading to the $I4/mmm$ space group confirmation. In some diffraction patterns, distortion of the spots along the c direction have been observed. They reflect the presence of stacking faults along this direction, as will be discussed in Section 3.4.

3.2. Neutron Diffraction

Neutron diffraction, which is very sensitive to oxygen localization, is the best tool to confirm the anionic arrangement. Structural refinement of the neutron diffraction pattern of $Nd_4Ni_3O_8$ unambiguously confirmed the T′ type atomic arrangement. Both T* type and T′ type arrangements were tested. Figure 3a provides a comparison of observed and calculated patterns, with an oxygen atom fixed in the apical position O4 of Fig. 1b, at about 2 Å of the nickel position (T* type arrangement). Figure 3b provides the best fit obtained with oxygen in position O5 of Fig. 1c (T′ type arrangement). There is thus no ambiguity that the real structural arrangement is actually the T′-type. Figure 4 provides a polyhedral representation of the refined crystal structure of the compound, and Tables 1 and 2 display the atomic positions and interatomic distances, respectively. The two nickel atoms in square planar coordination exhibit identical Ni–O distances, within the measurement accuracy. The two neodymium atoms in pseudocubic coordination have somewhat different types of environment. If the Nd1 site is rather symmetrically surrounded by oxygen (4×2.49 and 4×2.57 Å), the Nd2 site is not centered in its pseudocubic environment, with 4 oxygen at short distance (2.32 Å) and 4 at a longer distance (2.72 Å).

During the structural refinement, the presence of anisotropic broadening of reflections has been observed. A detailed analysis of the systematic broadening as a function of hkl led us to conclude that this was due to a size effect. The modeling of the anisotropic broadening involved the hypothesis (perfectly confirmed by electron microscopy as explained below) that the correlation length for coherent crystallites was finite along the c axis.

The simplest model is that the crystallites are platelets with an effective finite size along [001] (normal to the platelets) and infinite within the (001) plane.

The integral breadth (β_{hkl}, corrected for instrumental resolution), of a Bragg reflection for a small crystallite is given by the Scherrer formula:

$$\beta_{hkl} = \lambda / D_{hkl} \cos\theta,$$

where λ is the wavelength, θ is the Bragg angle, and D_{hkl} is the volume average (for all crystallites of the sample) of the diameters normal to the (hkl) planes. If D is the average thickness of the platelets, then $D = D_{hkl} \cos\alpha_{hkl}$, where α_{hkl} is the acute angle formed by the normal to the (hkl) planes and the normal to the platelets. If we assume that the broadening is mainly of lorentzian character, then the FWHM is given (in degrees) by

$$\mathrm{FWHM_L} = 360\lambda \cos\alpha_{hkl} / (\pi^2 D \cos\theta) = S_Z \cos\alpha_{hkl} / \cos\theta,$$

where S_Z is the parameter refined by FullProf, from which the average thickness, D, can be obtained. This Lorentzian broadening is added to the instrumental Lorentzian component that, combined with the Gaussian component, synthesize the experimental Voigt peak shape (approximated with the pseudo-Voigt function). This model explains perfectly the neutron diffraction pattern. The value obtained for the volume averaged thickness is $D = 550(24)$ Å. The precise nature of the defects giving rise to the lack of long-range coherence of crystallites along [001] can only be determined

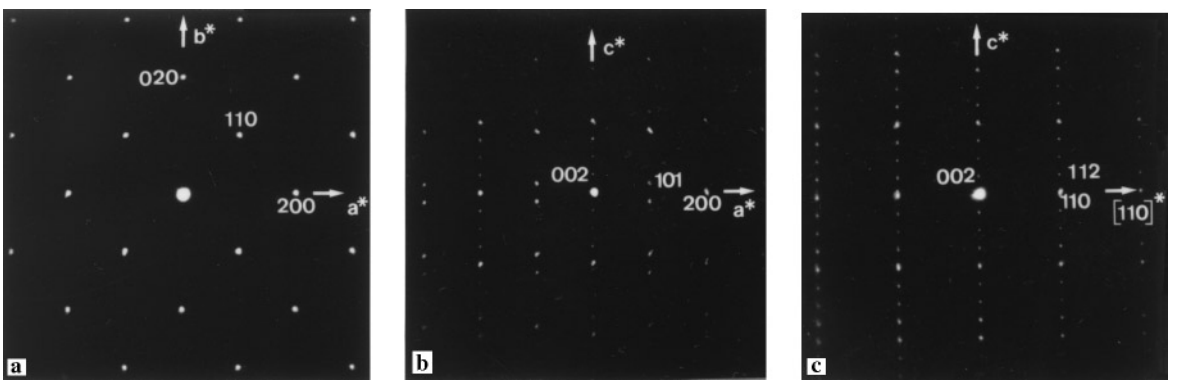

FIG. 2. Electron diffraction patterns of $Nd_4Ni_3O_8$ along [001] (a), [010] (b), and [1$\bar{1}$0] (c) zone axes.

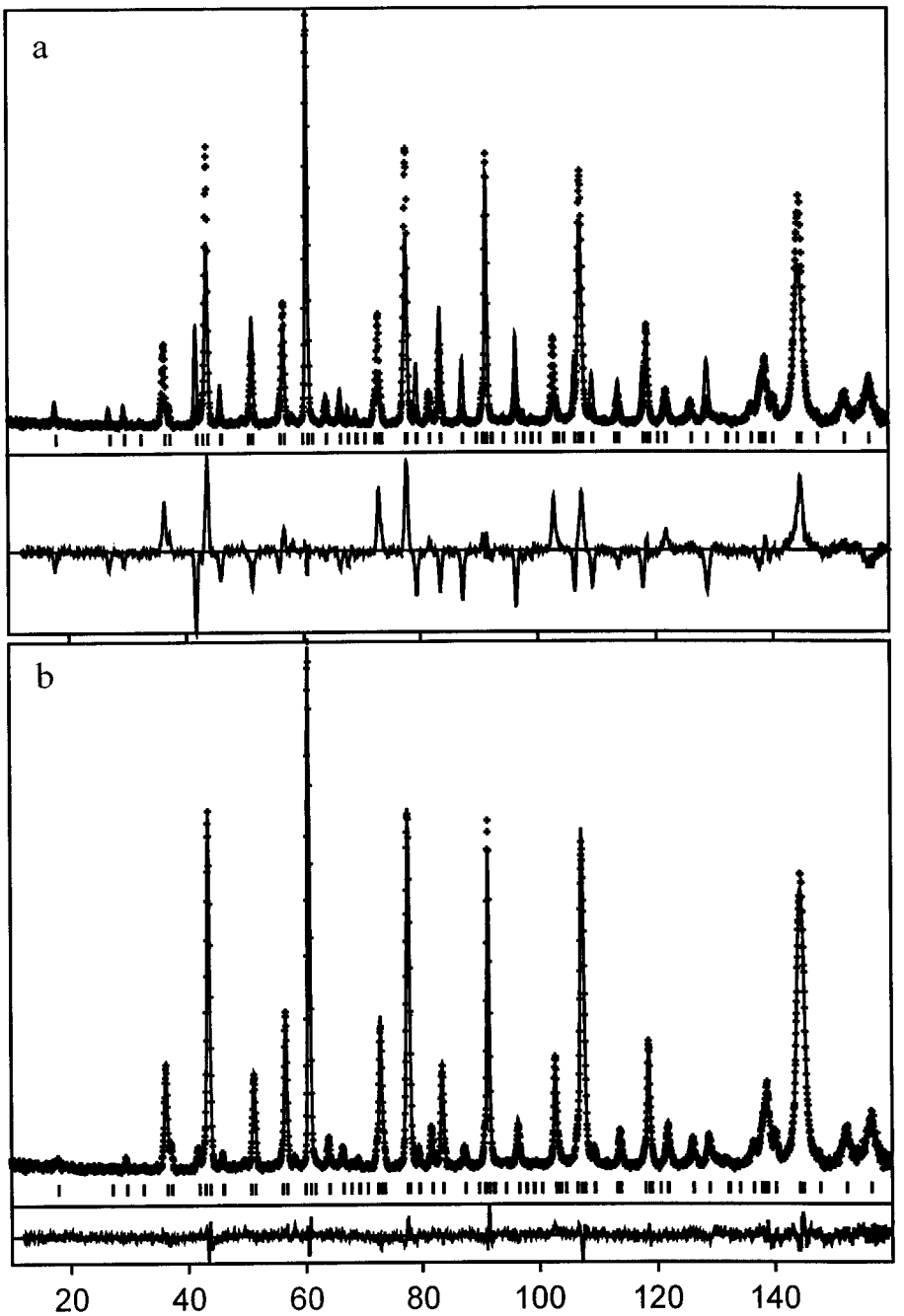

FIG. 3. Observed (crosses), calculated (lines), and difference (bottom) neutron diffraction patterns assuming (a) a T* type arrangement with oxygen atom O4 (see Fig. 1b) or (b) a T′ type arrangement with oxygen atom O5 (see Fig. 1c). Horizontal 2θ scale is in degrees.

with the help of high resolution electron microscopy (see Section 3.4).

3.3. High-Resolution Electron Microscopy of Regular Zones

HREM simulated images were calculated using the model determined by neutron diffraction and were compared to the experimental images of $Nd_4Ni_3O_8$, observed along the [010] and [$1\bar{1}0$] zone axes. Due to the atomic distribution in the structure, [$1\bar{1}0$] observations did not provide detailed information about the stacking of the layers.

The [010] orientation is best suited to visualize the layer stacking. Calculated through focus series fit well with the experimental images and permitted an interpretation of the observed contrasts. For different defocus values, the

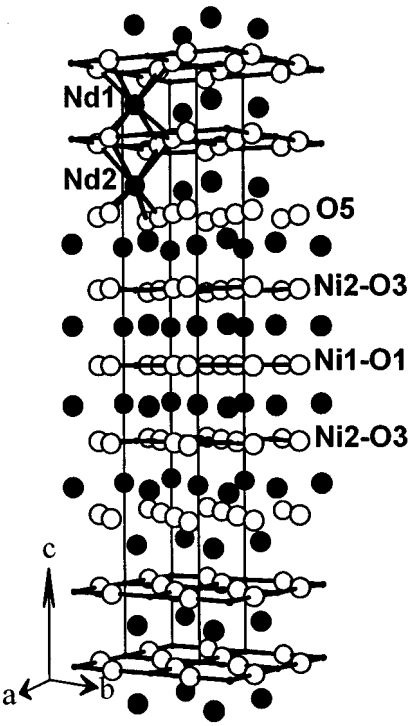

FIG. 4. The crystal structure of $Nd_4Ni_3O_8$ (atomic symbols: same as Fig. 1).

different sublattices can be imaged. Figure 5 exhibits two most typical images (experimental and calculated) of the $Nd_4Ni_3O_8$ structure for a thickness close to 30 Å.

TABLE 1
Crystal Structure of $Nd_4Ni_3O_8$ from Neutron Diffraction (z and B Values in Italic Type Are from X-ray Diffraction (Ref. (2))

Atom	Site	x	y	z	B (Å^2)
Nd1	4*e*	0	0	0.4342(1)	0.28(4)
				0.4339(1)	*0.49(3)*
Nd2	4*e*	0	0	0.2988(2)	0.28(4)
				0.2984(1)	*0.34(3)*
Ni1	2*a*	0	0	0	0.27(3)
					0.4(2)
Ni2	4*e*	0	0	0.1254(1)	0.27(3)
				0.1248(2)	*0.5(1)*
O1	4*c*	0	$\frac{1}{2}$	0	0.43(3)
					−0.1(4)
O3	8*g*	0	$\frac{1}{2}$	0.1267(1)	0.43(3)
				0.1250(4)	*0.8(3)*
O5	4*d*	0	$\frac{1}{2}$	$\frac{1}{4}$	0.43(3)
					0.9(5)

Note: Space group $I4/mmm$, $a = b = 3.9168(2)$ Å, $c = 25.322(2)$ Å. Refinement within the range $12° < 2\theta < 159.5°$, including 86 reflections (no excluded regions) with 24 refined parameters (including 6 background parameters). Thermal factors were constrained to be equal for sites with same elements. Conventional reliability factors: $R_p = 0.125$, $R_{wp} = 0.108$, $\chi^2 = 2.81$, $R_{Bragg} = 0.043$, $R_F = 0.037$.

TABLE 2
Interatomic Distances and Angles in $Nd_4Ni_3O_8$

Nd1–O3	$4 \times 2.493(3)$ Å	Ni1–O1	$4 \times 1.958(1)$ Å
–O1	$4 \times 2.572(2)$ Å	Ni2–O3	$4 \times 1.959(1)$ Å
Nd2–O5	$4 \times 2.316(2)$ Å	O1–Ni1–O1	180°
–O3	$4 \times 2.718(3)$ Å	O3–Ni2–O3	178.0(2)°

On the photographs of Figs. 5a and 6, which were obtained for a defocus value of −850 Å, all cations appear as white, more or less intense dots. Figure 5b corresponds to a defocus value of −550 Å, close to Scherzer: white dots are representative of the lowest electronic densities and all atoms appear in black (in fact, the sublattice of white dots is representative, with a translation of $a/2$, of the neodymium atoms distribution in the structure).

The contrast observed on Figs. 5a and 6, with gray zigzag ribbons neighboring three intense white dots and light gray dots characteristics of the Ni and Nd atoms, respectively, seems to be characteristic of a T′ type structure (Fig. 1c); indeed, as in the neutron study, we calculated a through focus series, using a model with a T* type arrangment of atoms in the structure ((4), Fig. 1b). These series did not fit with the through-focus observed images obtained on the $Nd_4Ni_3O_8$ compound. Moreover, the simultaneous presence of the two characteristic contrasts of Fig. 5 was never clearly in evidence in this series.

Thus, the Nd–O fluorite type layer in between triple Ni–O layers where nickel atoms appear as intense white dots is clearly substantiated by the gray zigzag ribbons pointed by black arrows on Fig. 6.

3.4. *Defects in $Nd_4Ni_3O_8$*

The existence of $R_4Ni_3O_8$ (R = La, Pr, Nd) series suggests an outline for a new structural series with formula $A_{n+1}B_nO_{2n+2}$, where n represents the number of adjacent square planar NiO_2 layers (2). Even if attempts to prepare other members of these series were unsuccessful up to now, we observed defects in the $n = 3$ compound $Nd_4Ni_3O_8$ with $n < 3$ (often) and with $n > 3$ (rarely).

Defects shown on Fig 7a with the typical contrast of Fig. 5b are stacking faults which correspond to an irregular intergrowth of single and double layers in a mainly triple-layer matrix. This type of defect has already been observed by other authors in the oxidized phases $La_3Ni_2O_7$ and in $La_4Ni_3O_{10}$ (8, 9).

A model of these defects is proposed on Fig. 7b, together with the equivalent defect in the parent oxidized phase on Fig. 7c. Contrary to what happens in the triple-layer slabs, it is very unlikely for nickel coordination to be lowered to four in single and double layers during reduction. In the nickelates, contrary to the cuprates, the single layer type

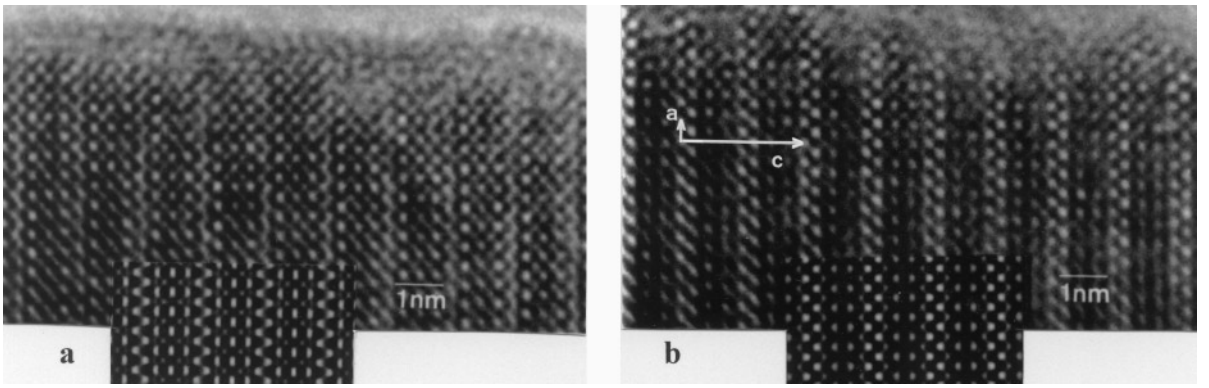

FIG. 5. Characteristic HREM experimental [010] images of $Nd_4Ni_3O_8$, with calculated images in insert (thickness = 31 Å, $C_s = 1.0$); defocus values, (a) -850 Å; (b) -550 Å. The scale bars are parallel to the c axis.

structure exists only in the T type arrangement, and reduction cannot play a determinant role in the process, since both T type and T′ type structures have the same formulation. For double layers, the situation is less clear. Zhang *et al*. have studied the reduction of $La_3Ni_2O_7$ under diluted hydrogen (10). They found, as we did (2), that reduction is only partial, leading to composition $La_3Ni_2O_{6.35}$. Their results suggest that 65% of vacancies are located on the oxygen site in between two adjacent perovskite layers: it is the hypothesis that we assumed in our model.

An $n = 6$ defect in an $n = 3$ matrix is presented in Fig. 8a. Here a propagation through the crystal of the defect composed by six Ni–O layers in square planar coordination can be seen.

A model of this defect is proposed on Fig. 8b, together with its counterpart in the original oxidized phase (Fig. 8c). The defect can be viewed as somewhat equivalent to two parallel edge dislocations within a perovskite or infinite layer (in fact, nine-layer) structure, with the extra inserted semi-planes built up from rare earth and oxygen atoms. In the reduced phase, nickel coordination higher than four is locally possible around the dislocation lines.

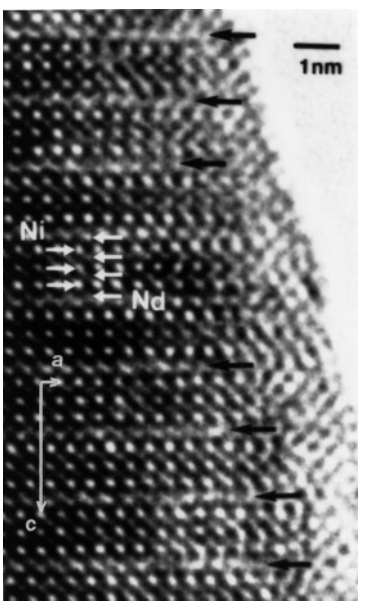

FIG. 6. [010] HREM image where all cations can be imaged as white dots (defocus value -850 Å). Nickel atoms appear as intense white dots. Black arrows (parallel to the a axis) show zigzag ribbons characteristic of Nd–O fluorite type layers.

4. SUMMARY AND CONCLUSION

The present study confirms that structural arrangements similar to those found in superconducting cuprates can be stabilised in other transition metal oxides by using indirect synthesis routes. We have confirmed here that the reduction of $R_4Ni_3O_{10}$ under hydrogen leads to the loss of two oxygen atoms, and the migration of two others in such a way that it leaves nickel atoms in square planar coordination.

The reduced phases $R_4Ni_3O_8$ belong to a new structural series $A_{n+1}B_nO_{2n+2}$ which can be closely related to the Ruddlesden–Popper series (2). As the Ruddlesden–Popper series $A_{n+1}B_nO_{3n+1}$ can be reformulated as the intergrowth of n perovskite layers with one rock salt type layer ($n[ABO_3] + [AO]$), the new series can be considered as the stacking of n layers of the "infinite layer" type and one fluorite-type layer ($n[ABO_2] + [AO_2]$). Both series can be gathered in a structural "superfamily" with composition $A_{n+1}B_nO_{(2+p)n+2-p}$, where n represents the number of successive $[BO_2]$ layers, and p the presence ($p = 1$) or absence ($p = 0$) of apical oxygen atoms (11). Each member of this super-family can be specified by the corresponding (n, p) couple (see Fig. 9). The two original members of the double series, (1, 0) and (1, 1), which have the same formulation A_2BO_4, correspond to T′ type and T type structures, the

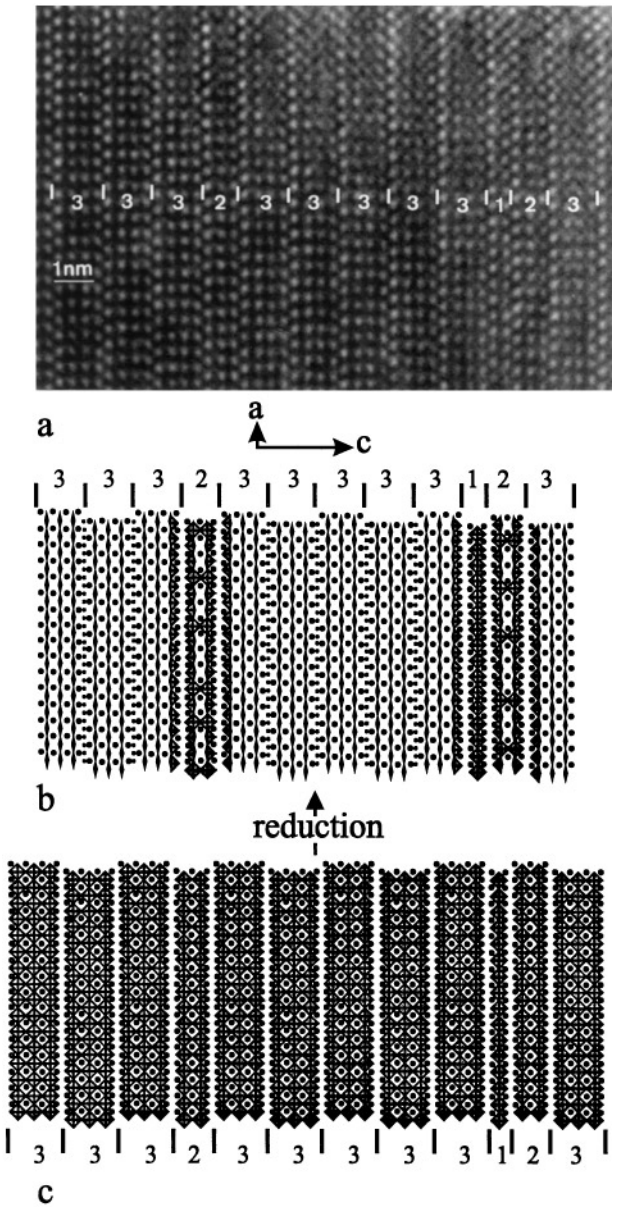

FIG. 7. Stacking faults with single and double-layer defects, (a) as observed by HREM along the [010] direction, (b) model of the previous defects (see text for details), (c) model of the same defects in the parent oxidized phase $Nd_4Ni_3O_{10}$. (Black flat lozenges, triangles, and squares represent $[NiO_4]$ square planes, $[NiO_5]$ pyramids, and $[NiO_6]$ octahedra, respectively, while dots and crosses indicate Nd and O atoms, respectively.)

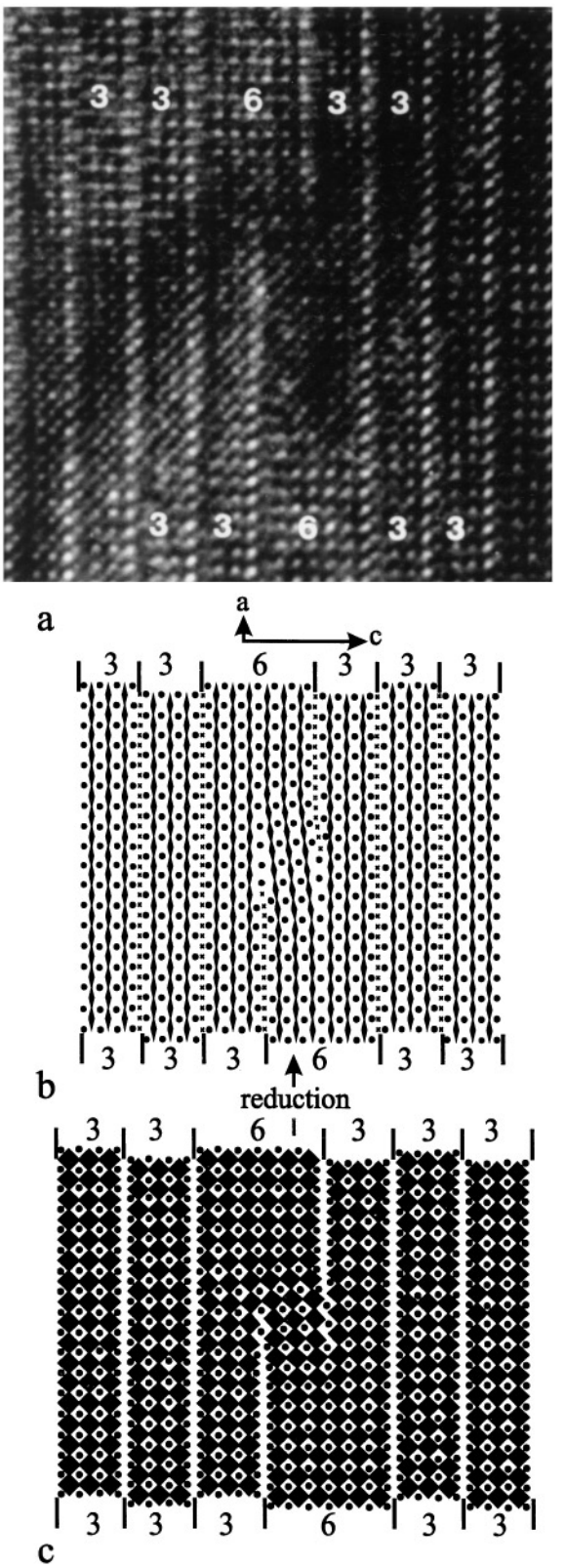

FIG. 8. A six-layer defect in a triple-layer matrix, (a) as observed by HREM along the [010] direction, (b) model of the previous defect, (c) model of the same defect in the parent oxidized phase $Nd_4Ni_3O_{10}$. (See legend to Fig. 7.)

prototypical structures of electron and hole-doped single-layer superconducting cuprates, respectively. The other end members are $(\infty, 0)$ and $(\infty, 1)$, which represent the infinite-layer type and perovskite structures, respectively. The infinite-layer type structure has already been encountered in cuprates $Ca_{1-x}Sr_xCuO_2$ (12) and $Sr_{1-x}R_xCuO_2$ (13) and nickelate $LaNiO_2$ (14). Structure $(2, 0)$ has not yet been observed: $La_2SrCu_2O_6$ (15) falls in the same class, but its

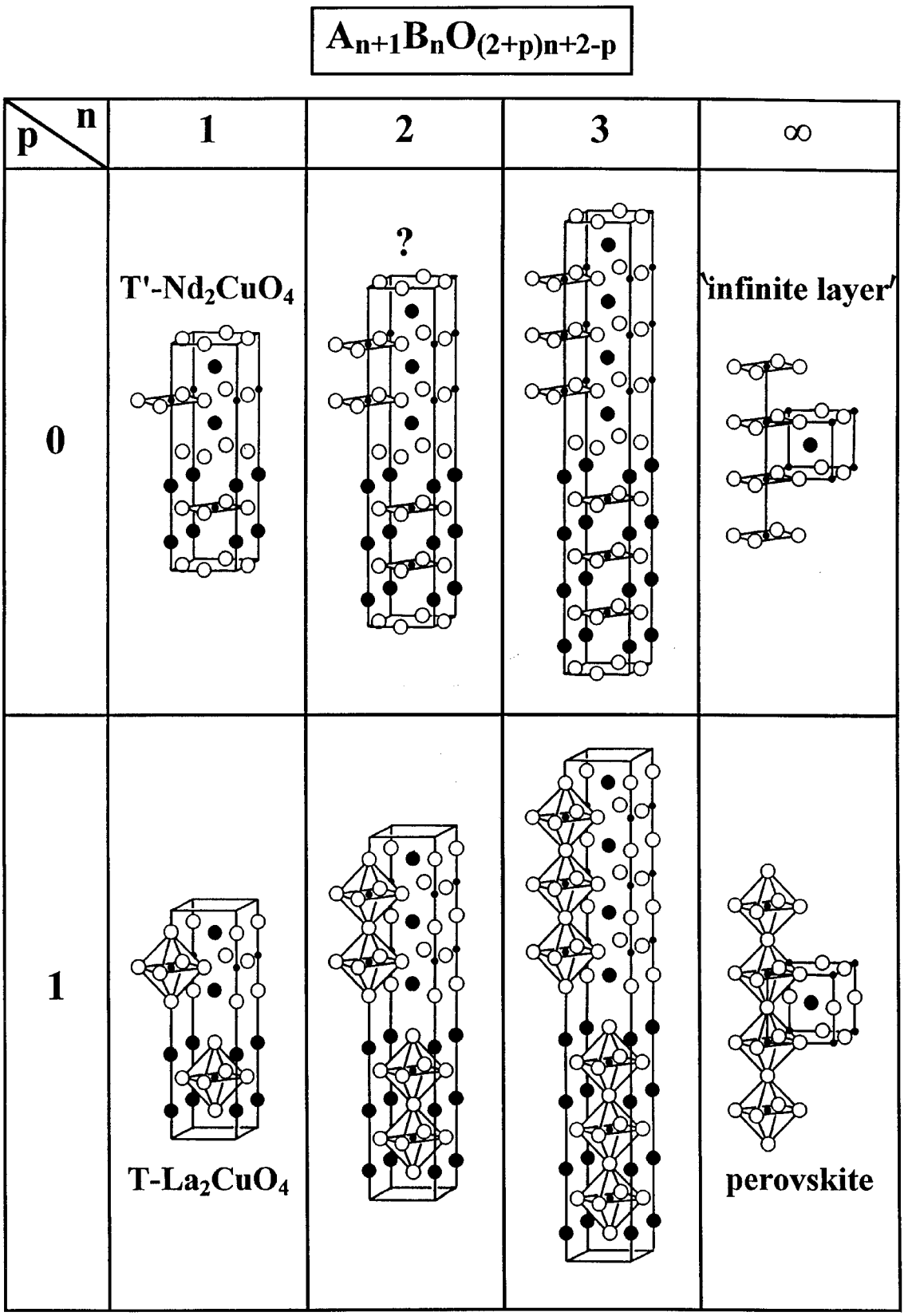

FIG. 9. Classification of layered oxides as a function of the number n of adjacent ABO_2 ($p = 0$) or ABO_3 ($p = 1$) layers in between fluorite or rock salt type layers, respectively. The bottom series ($p = 1$) corresponds to the Ruddlesden–Popper series.

structure exhibits apical oxygen, while reduction of $La_3Ni_2O_7$, as mentioned earlier, is only partial with $0 < p < 1$. In general, intermediate values of p between 0 and 1 are possible for each member of the series, with vacancies more or less well ordered on the oxygen lattice, as for instance in reduced perovskites $ABO_{2.5}$ and in $La_4Ni_3O_9$ (2). Apart from the end members $n = 1$ and $n = \infty$, the only known members of the $(n, 0)$ series are the nickelates $R_4Ni_3O_8$.

Finally, neutron and electron diffraction has permitted the determination of the coherence lengths inside multidomain crystals, and the modelling of two different types of defects observed in $Nd_4Ni_3O_8$.

REFERENCES

1. Y. Tokura, H. Takagi, H. Watabe, H. Matsubara, S. Uchida, K. Hiraga, T. Oku, T. Mochiku, and H. Asano, *Phys. Rev. B.* **40,** 2568 (1989).
2. P. Lacorre, *J. Solid State Chem.* **97,** 495 (1992).
3. S. N. Ruddlesden and P. Popper, *Acta Crystallogr.* **11,** 54 (1958).
4. A. M. Guloy, B. A. Scott, and R. A. Figat, *J. Solid State Chem.* **113,** 54 (1994).
5. P. A. Stadelman, *Ultramicroscopy* **21,** 131 (1987).
6. J. Rodriguez-Carvajal, "FullProf: A Program for Rietveld Refinement and Pattern Matching Analysis." Abstracts of the Satellite Meeting on Powder Diffraction of the XV Congress of the IUCr, p. 127, Toulouse, France, 1990.
7. P. Thompson, D. E. Cox, J. B. Hastings, *J. Appl. Crystallogr.* **20,** 79 (1987).
8. J. Drennan, C. P. Tavares, and B. C. H. Steele, *Mater. Res. Bull.* **17,** 621 (1982).
9. R. A. Mohan Ram, L. Ganapathi, P. Ganguly, and C. N. R. Rao, *J. Solid State Chem.* **63,** 139 (1986).
10. Z. Zhang, M. Greenblatt, and J. B. Goodenough, *J. Solid State Chem.* **108,** 402 (1994).
11. P. Lacorre, *Act. Chim.* **2,** 16 (March 1995).
12. T. Siegrist, S. M. Zahurak, D. W. Murphy, and R. S. Roth, *Nature* **334,** 231 (1988).
13. M. G. Smith, A. Manthiram, J. Zhou, J. B. Goodenough, and J. T. Markert, *Nature* **351,** 549 (1991).
14. P. Levitz, M. Crespin, and L. Gatineau, *J. Chem. Soc., Faraday Trans. 2,* **79,** 1195 (1983).
15. N. Nguyen, L. Er-Rakho, C. Michel, J. Choisnet, and B. Raveau, *Mater. Res. Bull.* **15,** 891 (1980).